Revista Ciencia e Ingeniería Neogranadina 2024 julio - diciembre Vol. 34(2) ISSN: 0124-8170 · e-ISSN: 1909-7735 ■ pp. 63-75

Editorial Neogranadina

DOI: https://doi.org/10.18359/rcin.7276

CC BY NC ND

Computational Modeling of Light Scattering in Polymer Nanoparticles for Optical Characterization*

Agni Puentes Ossa[a] ■ Diego Julian Rodriguez Patarroyo[b] ■ Julian Andres Salamanca Bernal[c]

Abstract: The scattering of light by polymeric nanoparticles is a crucial phenomenon in various applications, ranging from nanomedicine to nanophononics. This study introduces a theoretical framework for differentiating between absorption and scattering spectra in light interactions with these nanoparticles. Characteristic spectral data of nanoparticles synthesized via the reprecipitation method and suspended in an aqueous medium analyzed under electromagnetic radiation. These nanoparticles exhibit two primary optical phenomena: absorption and scattering. To fully understand their optical response, it is essential to separate these phenomena. This study established a relationship between wavelength variation, nanoparticle size, and radiation loss due to scattering in an aqueous medium. Additionally, we calculated extinction efficiency and extinction factors as functions of wavelength, taking into account variations in nanoparticle radii and refractive indices.

Key words: Polymer nanoparticles; Mie theory; light scattering; numerical modelling; spectral partitioning

Recibido: 06/04/2024 **Aceptado:** 22/04/2024 **Disponible en línea:** 29/10/2024

Cómo citar: Puentes Ossa, Agni, Salamanca Bernal, J. A., & Rodriguez, D. J. (2024). Modelado Computacional De La Dispersión De Luz En Nanopartículas De Polímero Para Caracterización Óptica. *Ciencia E Ingeniería Neogranadina, 34*(2), 63–75. https://doi.org/10.18359/Rcin.7276

* Research Article.

a Master's in Electrical Engineering, Bachelor's in Physics, Universidad Franciso José de Caldas, Bogotá, Colombia.
Email: ampuenteso@udistrital.edu.co; ORCID: https://orcid.org/0000-0002-0714-5355

b Ph.D. in Engineering – Materials Science and Technology, Master's in Physics, Universidad Franciso José de Caldas, Bogotá, Colombia.
Email: djrodriguezp@udistrital.edu.copH; ORCID: https://orcid.org/0000-0002-4907-5674

c Ph.D in Applied Physics, Master's in Physics, Bachelor's in Physics. Universidad Franciso José de Caldas, Bogotá, Colombia.
Email: jasalamanca@udistrital.edu.co; ORCID: https://orcid.org/0000-0001-8378-4215

Modelado Computacional de la Dispersión de Luz en Nanopartículas de Polímero para Caracterización Óptica

Resumen: La dispersión de la luz por nanopartículas poliméricas es un fenómeno crucial en diversas aplicaciones, desde nanomedicina hasta nano fotónica. Este trabajo introduce un marco teórico para distinguir entre los espectros de absorción y dispersión en las interacciones de la luz con estas nanopartículas. Datos espectrales característicos de nanopartículas, sintetizadas mediante el método de re-precipitación y suspendidas en un medio acuoso, fueron analizados bajo radiación electromagnética. Estas nanopartículas exhiben dos fenómenos ópticos primarios: absorción y dispersión, los cuales deben separarse para comprender completamente su respuesta óptica. Se estableció una conexión entre la variación de longitud de onda, el tamaño de la nanopartícula y la pérdida de radiación atribuible a la dispersión en un medio acuoso. Además, se realizaron cálculos del factor de eficiencia de extinción y factores de extinción en función de la longitud de onda, teniendo en cuenta las variaciones en los radios de las nanopartículas e índices de refracción.

Palabras clave: nanopartículas poliméricas; teoría de Mie; dispersión de luz; modelo numérico; división de espectro

Modelagem computacional da dispersão da luz em nanopartículas de polímero para caracterização óptica

Resumo: A dispersão da luz por nanopartículas poliméricas é um fenômeno crucial em diversas aplicações, desde a nanomedicina até a nanofotônica. Este trabalho introduz um marco teóricio para distinguir entre os espectros de absorção e dispersão nas interações da luz com essas nanopartículas. Dados espectrais característicos de nanopartículas, sintetizadas pelo método de reprecipitação e suspensas em meio aquoso, sob radiação eletromagnética. Essas nanopartículas exibem dois fenômenos ópticos primários: absorção e dispersão, os quais precisam ser separados para uma compreensão completa de sua resposta óptica. Estabeleceu-se uma conexão entre a variação do comprimento de onda, o tamanho da nanopartícula e a perda de radiação atribuída à dispersão em meio aquoso. Além disso, foram realizados cálculos do fator de eficiência de extinção e dos fatores de extinção em função da longitude de onda, considerando as variações nos raios das nanopartículas e nos índices de refração.

Palavras-chave: nanopartículas poliméricas; teoria de Mie; dispersão de luz; modelo numérico; divisão de espectro

Introduction

Investigations into the optical response of nanoparticles have prioritized the development of theoretical frameworks to elucidate their interactions with electromagnetic radiation in the visible range. In particular, the scattering spectra resulting from light-nanoparticle interactions have been analyzed for various nanoparticle types. This study focuses on Polymeric Nanoparticles (NPPs). To understand the optical response of NPPs, it is crucial to distinguish between absorption and scattering spectra during light interactions.

Mathematical models that account for NPP-specific phenomena, such as anisotropic basis functions and heterogeneity, facilitate the estimation of classical radiation loss processes.

Gustav Mie's solution, the first complete spherical scattering theory, provides a description of the interaction between a plane wave and a spherical dielectric [1-5]. Adaptation of this theory and other radiation models, such as anisotropic basis functions and heterogeneity [6-9], by inputting specific parameters, allows the association of observed scattering phenomena with irradiated NPPs. Mie solutions are also used to study electromagnetic radiation interactions with the atmosphere particularly to quantify and determine atmospheric aerosol distributions on Earth and other planets [10]. However, this study focuses on parameters specific to NPPs designed for drug delivery.

As a result, two spectra are obtained from different sources. The first relates to the absorption processes of electromagnetic radiation due to morphological characteristics, polymer arrangement, and configuration. The second pertains to the dispersive light response, which depends on the size of the NPP and the wavelength of the interacting radiation.

It is important to consider the classification of NPPs based on the materials used for their core and shell/cover. Toxicological engineering generally classifies nanoparticles [11-12]. First, monolayer or two-dimensional multilayer carbon nanotubes range from 2 to 50 nm, with lengths exceeding 100 nm. Second, fullerenes serve as water-soluble organic spherical cages. Third, dendrimers have sizes as small as 10 nm, which limits the incorporation of molecules. Finally, three-dimensional spherical semiconductor nanocrystals (1-10 nm QDs or quantum dots) range from 2.5 to 100 nm, as do gold nanoparticles/nanocapsules (1-100 nm), and silica nanoparticles of various shapes and sizes [13-15].

For NPPs, materials include lipid, protein, natural, semi-synthetic, and synthetic polymers. For example, NPPs could be hyperbranched polymer dendrimers with applications in biology and medicine [11,16,17].

The use of NPPs in various applications is primarily due to their polymeric base, which allows them to be dispersed in any material matrix. Additionally, they can be biofunctionalized, conjugated, and coated, making them suitable for targeted and controlled delivery. This increases their value as biomarkers and improves their stability, solubility, and cytocompatibility. The NPPs studied are nanospheres prepared using a fluorene monomer-polymer conjugate encapsulated in silica nanoparticles to enhance biocompatibility.

However, the production of nanoparticles presents challenges such as reproducibility, scalability and, cost effectiveness. Several methods have been developed to overcome these limitations. One common method is reprecipitation, which involves the precipitation of a poorly soluble material from a non-solvent solution, allowing the synthesis of monodisperse nanoparticles with controlled size and shape [18]. Other methods include emulsion polymerization, microemulsion, and electrospinning [18-19], each of which its own advantages and disadvantages, selected based on specific applications and desired nanoparticle properties.

In the emulsion/evaporation method, an emulsion is formed by adding a polymer non-solvent to the system. This process leads to polymer precipitation and nanoparticle formation. A variant of this method, known as double or triple emulsion, involves performing two or three emulsification steps to increase encapsulation efficiency. Emulsification diffusion uses a water-in-oil emulsion, where the water phase contains the drug to be encapsulated. The solvent in the oil phase diffuses into the water phase, causing the polymer to precipitate and form nanoparticles. Nanoprecipitation involves adding a non-solvent to a

polymer solution, which results in polymer precipitation and the formation of nanoparticles. These methods are widely used in the manufacture of various types of nanoparticles, including NPPs [11, 12, 20, 21].

The preparation method can affect NPP properties such as size, shape, and surface chemistry, which, in turn, can influence their biological interactions and applications. Selecting the appropriate preparation method is critical to obtaining NPPs with the desired properties and functions. Additionally, characterizing NPPs is essential to confirm their physicochemical properties, stability, and toxicity, among other parameters. Common techniques used to characterize NPPs include dynamic light scattering, transmission electron microscopy, X-ray diffraction. Fourier transform infrared spectroscopy, and UV- Vis spectroscopy, among others [11, 13, 22].

The study of absorbed radiation and various wave phenomena occurring when NPPs are irradiated are irradiated in an aqueous medium involves examining experimental absorption data. In some cases, the focus is on the sensitivity of the nanoparticle to light [5, 23, 24] to generate a scattering curve based on Mie solutions. These solutions use experimental data as a reference [25]. This approach represents a classical solution, limited to the optical phenomenon of light scattering on NPPs.

1. Methods

In an attempt to obtain the characteristic spectra of light scattering through NPPs using the numerical model of Mie theory, a dataset from Aparicio, et al. [25] was selected. This dataset includes absorption spectra obtained from polymeric nanoparticles synthesized by the reprecipitation method with THF solutions at concentrations ranging from 0.08 mM to 98 mM. The synthesized nanoparticles were suspended in an aqueous medium, with an average size ranging from 19 to 125 nm and a refractive index of 1.4. The numerical model was fitted to the selected dataset based on the size trends discovered by Ramos et al. To initially test the model, the sample was limited to certain values, and the decay of the curves was observed.

This study presents a computational model that simulates the light scattering behavior of polymer nanoparticles immersed in an aqueous medium, focusing on nanometric sizes. The model, based on Mie theory, calculates the extinction efficiency factor and the extinction factors as a functions of wavelength for different nanoparticle radii.

The resulting spectra from this theory show a strong relationship with the refractive index, including both its real and imaginary components. In scenarios where the imaginary part of the refractive index is zero, the primary interference maximum approximately corresponds to the nanoparticle diameter and is accompanied by secondary maxima. As the imaginary part of the refractive index increases, the amplitude of the secondary maxima decreases. For larger particle radii, the extinction factor is higher due to the increased interaction between the material and the radiation, while the extinction efficiency factor retains similar behavior.

This computational approach provides a way to separate scattering and absorption spectra using theoretical methods, potentially replacing the empirical methods currently in use. Consequently, this research contributes to the advancement of optical characterization techniques for polymer nanoparticles and offers a solid foundation for further investigation and development in this field.

In this research, only selected combinations of parameters are analyzed, as the focus is on examining the light scattering behavior of specific cases presented in the Results and Discussion section.

1.1 Mie Theory: Mathematical model

The initial setup for the simulation involves a collection of polymeric nanoparticles with spherical geometry and dielectric properties, represented by a permittivity value of ϵ. Electromagnetic radiation is applied to the system with incident electric and magnetic fields, E_{inc} and H_{inc}, respectively, satisfying the relation $B=\mu H$. The scattered light fields, denoted by E_{esp} and H_{sct} (sct =scattering), are produced by the medium with permittivity ϵ_1, as depicted in *Figure* 1.

Figure 1. The scattering of light by an arbitrary particle is illustrated, showing the incident electric field, the scattering field, and the scattering field at large distances. Both polarization directions are visible, one contained in the scattering plane and the other perpendicular to the scattering plane. 1.1.1 Mie solution.

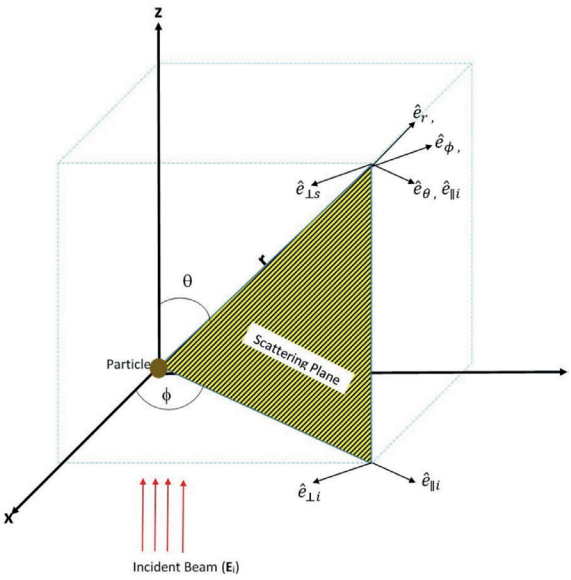

***Source*:** The authors.

It is well known that the behavior of electromagnetic waves in a given system must adhere to Maxwell's wave equations. Specifically, it is assumed that the electric field $\vec{E}$ and the magnetic field $\vec{H}$ in a linear, homogeneous, isotropic medium must satisfy the wave equation given in (1).

$$\nabla^2\vec{E} + k^2\vec{E} = 0 \qquad (1)$$

$$\nabla^2\vec{H} + k^2\vec{H} = 0$$

To simplify the problem, a vector field $\vec{M}$ is constructed as a function of a scalar function ψ and a constant vector $\vec{c}$, as shown in (2).

$$\vec{M} = \nabla \times (\vec{c}\psi) \qquad (2)$$

It satisfies (1) if and only if

$$\nabla^2\psi + k^2\psi = 0 \qquad (3)$$

Another vector function can be constructed from $\vec{M}$ that satisfies (1) and possesses all the properties of electromagnetic fields related to $\vec{M}$ [26]. This vector function has the form given in (4).

$$\vec{N} = \frac{\nabla\times\vec{M}}{k} \qquad (4)$$

Using this approach, the problem is reduced to finding solutions to a scalar wave equation. The scalar function ψ is commonly referred to as *the generating function of the harmonic vectors* $\vec{M}$ and $\vec{N}$. Furthermore, due to the spherical symmetry of the NPP in this problem, it is ensured that the solutions satisfy (1) in spherical polar coordinates. This allows us to rewrite $\vec{M}$ in the form of:

$$\vec{M} = \nabla \times (\vec{r}\psi) \qquad (5)$$

Moreover, the treatment of second-order differential equations in spherical coordinates allows the solution of the problem to be written as:

$$\psi(r,\theta,\phi) = R(r)\Theta(\theta)\Phi(\phi) \qquad (6)$$

According to the order of the equation, each of these functions must satisfy a second-order differential equation and be expressed as a linear combination of two solutions [26,27]. In the case of the function $\Phi(\phi)$, it has two types of solutions given by:

$$\Phi_e = \cos(m\phi),\ \Phi_o = \sin(m\phi) \qquad (7)$$

The subscripts e and o in this context refer to the even and odd characteristics of the function, respectively. For $\Theta(\theta)$, the solutions must be finite at θ=0 and θ=π. To satisfy this condition, we use the associated *Legendre functions* of the first kind, denoted by $P_n^m(\cos\theta)$, where n is the degree and m is the order [27]. These functions have the important property of being orthogonal with respect to their n subscripts. Additionally, when m=0, the associated Legendre functions reduce to *Legendre polynomials*, denoted by P_n.

The process of obtaining solutions for *R(r)* is considerably more complex. First, the associated differential equation is rewritten by introducing a dimensionless variable ρ=kr and defining the function Z=$R\sqrt{\rho}$. This transformation leads to a solution in the form of first and second kind of Bessel functions, denoted as J_ν and Y_ν, respectively. The order ν of these functions is half-integer and can be expressed as ν=n+1/2. Consequently, the desired functions are known as *spherical Bessel functions,* as given (8) and (9).

$$j_n(\rho) = \sqrt{\frac{\pi}{2\rho}} J_{n+1/2}(\rho) \qquad (8)$$

$$y_n(\rho) = \sqrt{\frac{\pi}{2\rho}} Y_{n+1/2}(\rho) \qquad (9)$$

The constant factor $\sqrt{\pi/2}$ is used to ensure that the recurrence relations work properly. However, changing the variable creates a problem as r approaches zero, since the limit tends to infinity.

Another important aspect to consider is that the behavior of the Bessel functions is not limited to real arguments only. In fact, their linear combinations can also form solutions to the radial differential equation. Such solutions are known as Bessel functions of the third kind, or *Hankel functions*. These functions are defined as:

$$h_n^{(1)} = j_n(\rho) + i y_n(\rho) \qquad (10)$$

$$h_n^{(2)} = j_n(\rho) - i y_n(\rho) \qquad (11)$$

From this repertoire of equations, one can rewrite (6) in the form:

$$\psi_{emn} = z_n(kr) P_n^m(\cos\theta)\cos(m\phi) \qquad (12)$$

$$\psi_{omn} = z_n(kr) P_n^m(\cos\theta)\sin(m\phi) \qquad (13)$$

By using any of the equations (10), (11), (9), or (8) for $z_n(kr)$ the resulting function can be expanded as an infinite series. This approach offers the advantage of allowing the construction of two functions for ψ, which can then be used to obtain two functions each for $\vec{M}$ and $\vec{N}$. These functions are denoted as $\vec{M}_{e,m,n}$, $\vec{M}_{o,m,n}$ and $\vec{N}_{e,m,n}$, $\vec{N}_{o,m,n}$ respectively.

1.2 The relation to the field

Having determined the possible wave function, it is essential to establish a relationship between $\vec{E}_1$ and the magnetic field. Starting with a plane wave polarized in X, written in spherical polar coordinates as in equation (14), four orthogonal vector functions were derived in the previous section.

$$\overrightarrow{E_\iota} = E_0 e^{ikr\cos\theta}\widehat{e_x} \qquad (14)$$

Due to the orthogonality relations of $\vec{M}_{e,m,n}$, $\vec{M}_{o,m,n}$ and $\vec{N}_{e,m,n}$, $\vec{N}_{o,m,n}$ [26], it can be written as:

$$\overrightarrow{E_\iota} = E_0 \sum_{n=1}^{\infty} i^n \frac{2n+1}{n(n+1)} \left(\vec{M}\, o1n^{(1)} - i\vec{N} e1n^{(1)}\right) \qquad (15)$$

The superscript (1) indicates that m=1, as observed in the subscripts of the functions. This notation appears when considering the internal field of the sphere or any other property related to the sphere. For instance, if v_1 refers to the permittivity of the sphere. With this clarification, the boundary equation can be written as:

$$\overrightarrow{E_\iota} = \overrightarrow{E_1} - \overrightarrow{E_s} \qquad (16)$$

when l is related to the incident electric field, equation (1) represents the electric field within the sphere, and s denotes the scattered electric field. By substituting $E_n = E_0 i^n \frac{2n+1}{n(n+1)}$, equation (15) becomes:

$$\overrightarrow{E_\iota} = \sum_{n=1}^{\infty} E_n \left(c_n \vec{M} o1n^{(1)} - i d_n \vec{N} e1n^{(1)}\right) \qquad (17)$$

The coefficients c_n and d_n define the behavior inside the sphere. With this information, only the analysis of the field outside the sphere, specifically the scattered field, remains. It should be noted that the solution function must exhibit good behavior at the origin. Typically, Hankel functions are chosen in this context, as only one of them is needed to expand the series [26]. Therefore, $\vec{E}_s$ is written as:

$$\overrightarrow{E_s} = \sum_{n=1}^{\infty} E_n \left(a_n \vec{N} e1n^{(3)} - i b_n \vec{M} o1n^{(3)}\right) \qquad (18)$$

Now, the superscript is (3), but m is still equal to (1). In this case, the superscript indicates that only the Hankel function $h_n^{(1)}$ has been chosen.

1.3 The dispersion coefficients

The previous calculations are important because they lead to the coefficients a_n and b_n, commonly known as the *dispersion coefficients*. To determine their values, it is assumed that the boundary conditions given in equation (16) are known and can be separated into each of the spherical variables.

To find these coefficients, two fundamental conditions are introduced. The first is the size parameter:

$$x = ka = \frac{2\pi N a}{\lambda} \qquad (19)$$

Here N represents the refractive index of the medium, and a is the radius of the particle. The second coefficient has been derived during the development process. Note that the refractive index consists of both real and imaginary:

$$N = n_r - in_i = n_r - i\frac{\alpha\lambda}{4\pi} \quad (20)$$

where a is known as the *absorption coefficient*. From this, the coefficients can be expressed as:

$$a_n = \frac{\mu m^2 j_n(mx)[xj_n(x)]' - \mu_1 j_n(x)[mxj_n(mx)]'}{\mu m^2 j_n(mx)\left[xh_n^{(1)}(x)\right]' - \mu_1 h_n^{(1)}(x)[mxj_n(mx)]'} \quad (21)$$

$$b_n = \frac{\mu_1 j_n(mx)[xj_n(x)]' - \mu j_n(x)[mxj_n(mx)]'}{\mu_1 j_n(mx)\left[xh_n^{(1)}(x)\right]' - \mu h_n^{(1)}(x)[mxj_n(mx)]'} \quad (22)$$

Since the denominators are very similar in structure, it can be inferred that the behavior of the scattered fields is a function of the normal modes. These coefficients are useful because several quantities involved in the experiment can be expressed as a function of them. In particular, the net ratio of energy passing through a surface of area A is defined as:

$$W_i = -\int_A \vec{S}_i \cdot \hat{e_r} d\vec{A} \quad (23)$$

where the index i corresponds to an imaginary surface used for radiation analysis, and $\vec{S}_i$ is the Poynting vector.

The total ratio of energy flowing over a surface A can be expressed as a balance between the absorbed and scattered energy ratios, as given in (24).

$$W_{ext} = W_{abs} + W_{sca} \quad (24)$$

The subscripts "*abs*" and "*sca*" refer to the absorbed and scattered energies by the particle, respectively. The extinction cross-section and the shape scattering can be expressed as:

$$C_{sca} = \frac{W_{sca}}{I_i} = \frac{2\pi}{k^2}\sum_{n=1}^{\infty}(2n+1)(|a_n|^2 + |b_n|^2) \quad (25)$$

$$C_{ext} = \frac{W_{ext}}{I_i} = \frac{2\pi}{k^2}\sum_{n=1}^{\infty}(2n+1)Re(a_n + b_n) \quad (26)$$

In this context, I_i refers to the *incident irradiance*. The advantage of this approach is that the $\vec{S}$ and the integrals are reduced to a summation of the coefficients a_n and b_n. Consequently, Q_{ext} can be determined by dividing the area.

1.4 Effective scattering sections and extinction factors

For the input parameter, the energy of the incident radiation perpendicular to the surface $\delta S'$ is assumed to be given by δE. Additionally, it is attenuated due to scattering and absorption by an amount δ_{ext}. Consequently, the effective extinction coefficient ias as given in (27) below [2, 10, 28].

$$Q_{ext} = \frac{C_{ext}}{A},\ Q_{abs} = \frac{C_{abs}}{A} \quad (27)$$

In the case of spheres, A is taken as the area of the circle.

2. Results

In this study, all nanoparticles are assumed to be spherical, with radii equal to the average of the synthesized NPPS, as reported by Aparicio et al., [25].

Figure 2 illustrates the behavior of the extinction efficiency factor Q_{ext} and the extinction cross-section factor C_{ext} in relation to the dispersive interaction between radiation and nanoparticles, considering the real part of the refractive index.

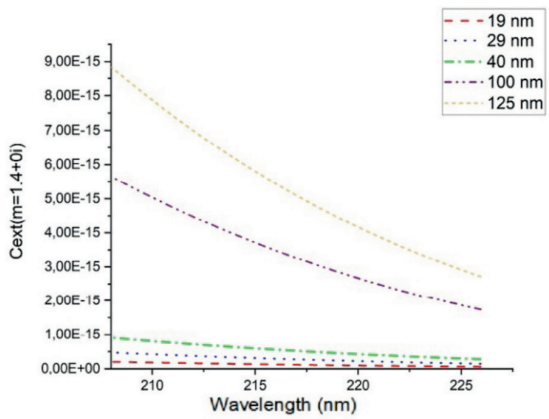

***Figure* 2.** Q_{ext} (left) and C_{ext} (right) for nanoparticles with sizes of 19, 29, 40, 100, and 125 nm, respectively, across wavelengths from 0 to 1000 nm, based on data from [25]. The particles are suspended in an aqueous medium with refractive index n=1.4.

The simulated numerical model used the size parameter $x = \frac{2\pi a n_m}{\lambda}$.

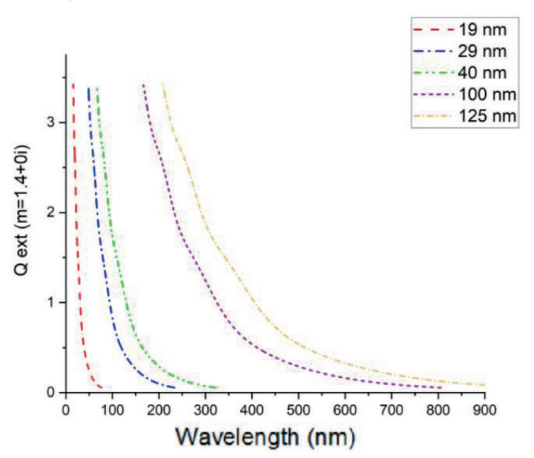

***Source*:** The authors.

For the study case, the relationship between Q_{ext}, (as given in (27)) and C_{ext}, as a function of wavelength and nanoparticle size (ranging from19 to 125 nm) was investigated.

It was observed that for sizes below 100 nm, the scattering reaches its maximum value in the ultraviolet range. Conversely, as the size increases beyond this range, the maxima shift towards the red end of the spectrum. Regarding the extinction factor, it was noted that for the two larger sizes, 100 and 125 nm, the extinction factor increases.

In *Figure* 3, the imaginary part of the refractive index was varied between 0 and 0.001, while the real part was fixed at n=1.4, for the aqueous medium. The nanoparticle size used was 100 nm, consistent with some parameters in the study by Ramos et al. A pronounced decrease in the visible sector of the spectrum was observed, attributed to the increase in the absorption factor at these wavelengths.

Figure 3. Q_{ext} (left) and C_{ext} (right) for m=1.4. Absorbance varies between 0 and 0.1 with a fixed particle size of 100 nm.

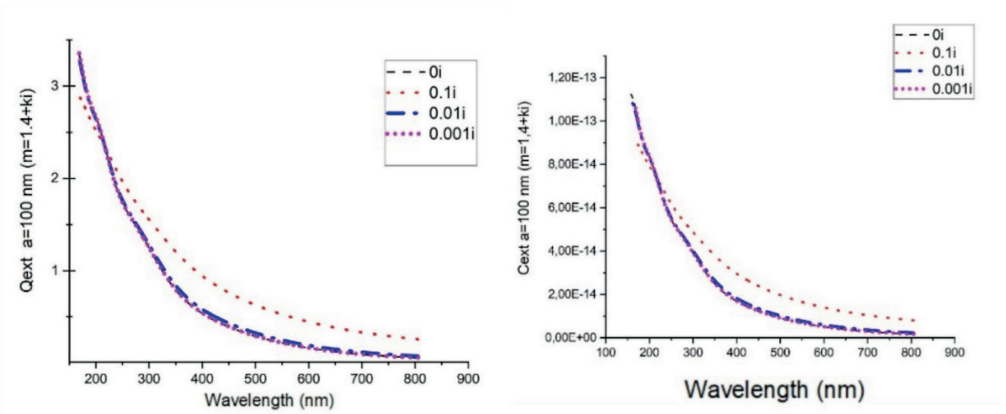

Source: The authors.

In *Figure* 4, the sizes of the nanoparticles were varied while the absorbance was set to 0.01. Compared to *Figure* 3, it is evident that the decay of the curve follows a similar trend in the wavelength ranges where the incident radiation is lost or extinguished. This indicates that, in both cases, the response for larger sizes, such as 100 nm, is maintained in the visible range.

***Figure* 4.** Left: Characteristic peaks of Q_{ext} for the imaginary part of the refractive index at i=0. Right: Characteristic peaks Q_{ext} for the refractive index with an imaginary part i=0.01.

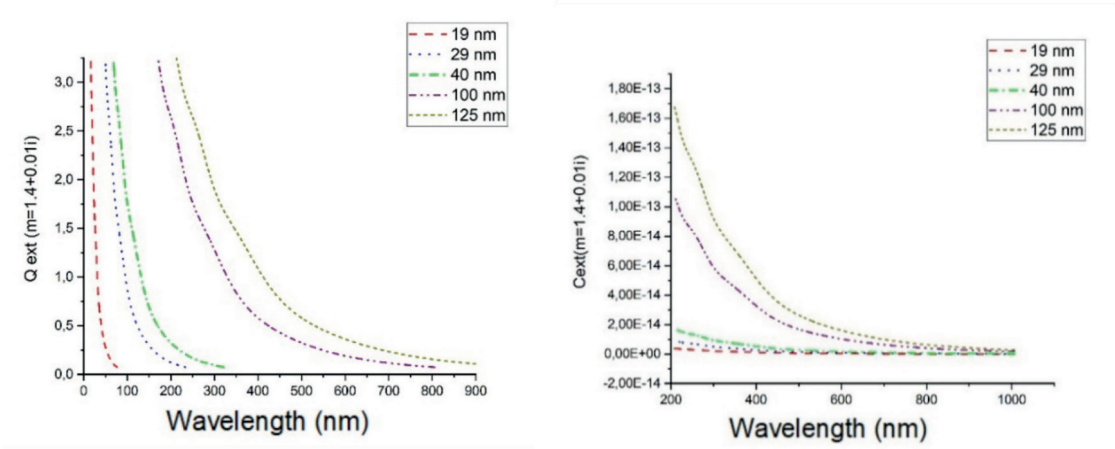

***Source*:** The authors.

A relationship between the extinction factor and the size of the nanoparticle is observed. The nanoparticle size range depends on the absorption factor (imaginary part of $\hat{n}$). By leaving ki, the slope of the curve in *Figure* 3 more clearly aligns with the expected wavelength ranges.

The highest values of Q_{ext} in *Figure* 4 are of equal magnitude and are proportional to the size parameter a of the nanoparticle. C_{ext}, as an extinction factor for larger nanoparticle sizes, has a radiation loss ratio of $2a$.

Additional refractive index values were evaluated to understand the effect of absorption. This helps in directly relating to with equations (27) and (21) when observing the behavior of the curve. The highest absorbance values are seen for intervals between 600 and 800 nm in *Figure*s 6 and 7.

Figure 5. Left: Characteristic peaks of Q_{ext} for the imaginary part of the refractive index at i=0. Right: Characteristic peaks of Q_{ext} for the refractive index with the imaginary part i=0.1.

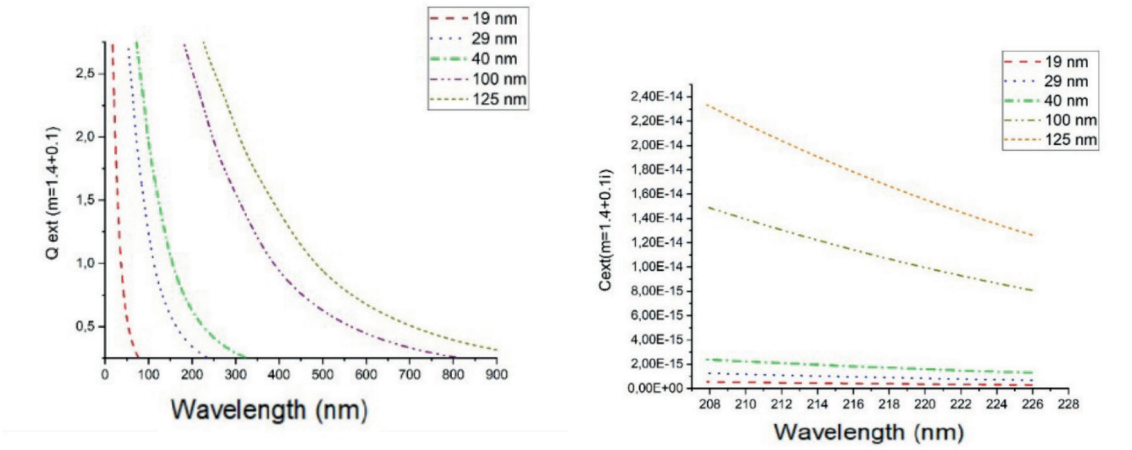

***Source*:** The authors.

Figure 5 illustrates the functional relationship between Q_{ext} and wavelength, showing a shift towards the visible region. C_{ext}, which is proportional to the radiation loss, also scales with the size of the nanoparticle. This behavior is particularly evident for particles ranging 100 to 125 nm.

***Figure* 6.** Left: Characteristic peaks of Q_{ext} for the imaginary part of the refractive index at i=0. Right: Characteristic peaks of Q_{ext} for the refractive index with the real part equal to 1.33.

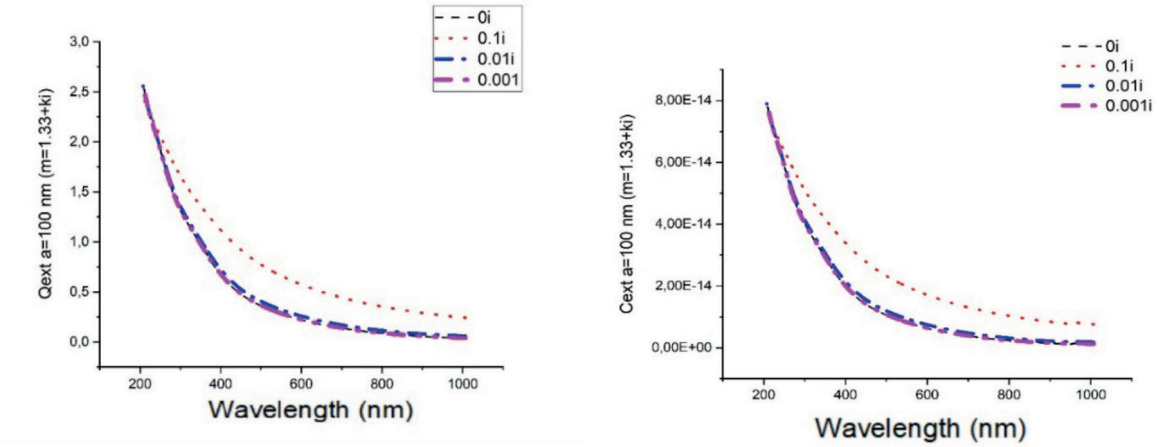

***Source*:** The authors.

Compared to *Figure* 4, the curve in *Figure 7* shows a smaller dip, indicating a correlation between the refractive index and the spreading process.

The curves obtained for each nanoparticle size illustrate the relationship between the wavelength extinction coefficients and the nanoparticle size (see *Figure*s 3, 4, and 5).

Maximum scattering occurs when the radiation wavelength is approximately twice the radius of the nanoparticle. Additionally, adjusting the imaginary component results in spectra with a redshift, aligning with the visible range for certain sizes.

For nanoparticles in different types of solution, results were obtained for various refractive indices, ranging between 1.33 and 1.5. *Figure*s 6 and 7 illustrate this radiation behavio.

Figure 7. Left: Characteristic peaks of Q_{ext} for the imaginary part of the refractive index at i=0. Right: Characteristic peaks b of Q_{ext} for the refractive index with the real part equal to 1.5.

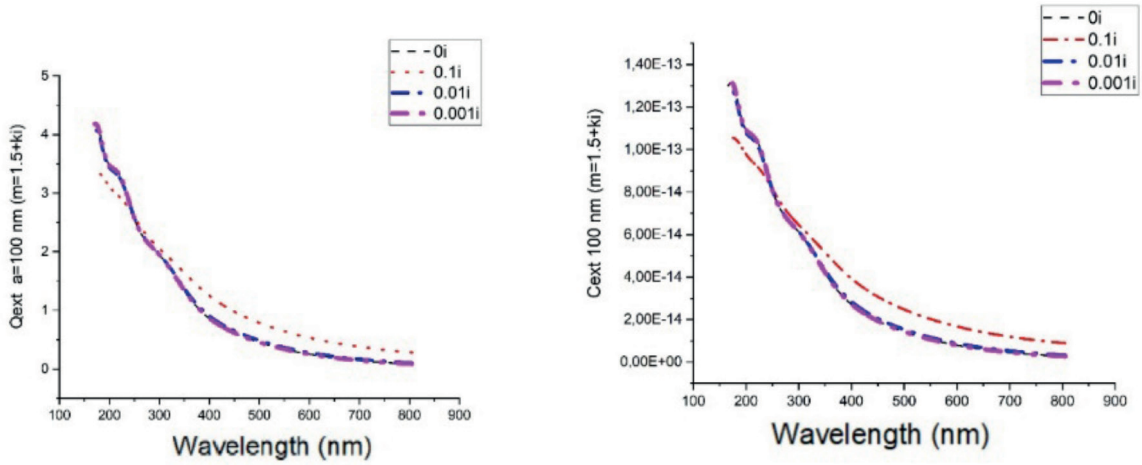

Source: The authors.

As the size of the nanoparticles increases, there is a corresponding rise in scattering. The extinction coefficient exhibits exponential decay and reaches its maximum in the ultraviolet range, as shown in *Figure* 7 (left) for a refractive index of 1.5. Comparing C_{ext}, which results from varying the imaginary part of the refractive index, reveals than an increase in *ki* leads to a higher extinction coefficient. This effect arises from the combination of dispersive effect and the material's absorption.

The results presented above cannot be directly compared to the experimental data from Aparicio [25] due to the approximations made in this study. Aparicio's synthesized particles displays size dispersion and non-spherical shapes, while this study assumes spherical nanoparticles of a unique size. However, the functional form of the scattering spectrum is consistent with experimental observations within specified ranges. The dependencies on size and refractive index are presented here also comparable to the experimental data.

3. Conclusion

This study introduces a computational model that simulates light scattering in polymer nanoparticles immersed in an aqueous medium, with a specific focus on nanometric sizes. The model, based on Mie theory, calculates both the extinction efficiency factor and extinction factors as a function of wavelength for various nanoparticle radii.

The spectra obtained demonstrate a strong correlation with the refractive index, including both its real and imaginary components. When the imaginary part of the refractive index is zero, the main interference peak closely corresponds to the nanoparticle diameter, accompanied by secondary peaks. As the imaginary part of the refractive index increases, the amplitude of the secondary peaks diminishes. For larger particle radii, the extinction factor increases due to enhanced interaction between the material and radiation, while the extinction efficiency factor shows similar behavior.

This computational approach offers a method for distinguishing between scattering and absorption spectra using theoretical models, potentially replacing the empirical methods currently in use. Consequently, this research significantly advances optical characterization techniques for polymer nanoparticles and lays a solid foundation for further exploration and development.

References

[1] Mishchenko, M.I.: Electromagnetic scattering by nonspherical particles: A tutorial review. Journal of Quantitative Spectroscopy and Radiative Transfer 8, 1699- 1719 (2009) DOI: https://doi.org/10.1016/j.jqsrt.2009.02.035

[2] Ghaforyan, H., Ebrahimzadeh, M., Bilankohi, S.M.: Study of the optical properties of nanoparticles using Mie theory. World Applied Programming 5(4), 79-82 (2015)

[3] Mock, J., Smith, D., Schultz, S.: Local refractive index dependence of plasmon resonance spectra from individual nanoparticles. Nano Letters 3 (2003) DOI: https://doi.org/10.1021/nl0340475

[4] Papoff, F., Hourahine, B.: Geometrical Mie theory for resonances in nanoparticles of any shape. Opt. Express 19 (2011) DOI: https://doi.org/10.1364/OE.19.021432

[5] Mie, G.: Beitr¨age zur optik tr¨uber medien, speziell kolloidaler metall¨osungen. Annalen der Physik 110

[6] Zhang, C., Wu, L., Zheng, C., al.: A differential theory of radiative transfer. ACM Transactions on Graphics 38, 1-16 (2019) DOI: https://doi.org/10.1145/3355089.3356522

[7] De La Rue, R.M.: Photonic crystals and photonic wires for a nanophotonic future? Applied Computational Electromagnetics Society Journal.Special Issue on Computational Bioelectromagnetics. 1, 282-284 (2004) DOI: https://doi.org/10.1109/ ICTON.2004.1360294

[8] Ohtsu, M., Kobayashi, K., Kawazoe, T.: Nanophotonics: Design, fabrication, and operation of nanometric devices using optical near fields. Selected Topics in Quantum Electronics, IEEE Journal of 8 (2002) DOI: https://doi.org/10.1109/JSTQE.2002.801738

[9] Johnson, J.M., Rahmat-Samii, V.: Genetic algorithms in engineering electromagnetics. IEEE Antennas and Propagation Magazine 39(7), 7-21 (1997) DOI: https://doi.org/10.1109/74.632992

[10] Solano-Reynoso, W.M., Acuña, J.R.: Esparcimiento de ondas electromagnéticas por microesferas dieléctricas. Revista de Investigación de Física 19 (2017) DOI: https://doi.org/10.15381/rif.v19i2.13558

[11] Bollhorst, T., Rezwan, K., Maas: Colloidal capsules: Nano- and microcapsules with colloidal particle shells. Chem. Soc. Rev. 46 (2017) DOI: https://doi.org/10.1039/C6CS00632A

[12] Urrejola, M.C., Soto, L.V., Zumarán, C.C., al.: Polymeric nanoparticle systems: Structure, elaboration methods, characteristics, properties, biofunctionalization and self-assembly layer by layer technologies. International Journal of Morphology 36, 1463-1471 (2018) DOI: https://doi.org/10.4067/S0717-95022018000401463

[13] Jamaludin, N., Abdul, S., Tan, T.: Natural Biomass as Carbon Sources for the Synthesis of Photoluminescent Carbon Dots, pp. 109-134 (2019) DOI: https://doi.org/10.1016/B978-0-12-815757-2.00005-X

[14] Joglekar, S., Gholap, H.M., Alegaonkar, P., al.: The interactions between cdte quantum dots and proteins: Understanding nano-bio interface. AIMS Journal 4, 209-222 (2017) DOI: https://doi.org/10.3934/matersci.2017.1.209

[15] Jaimes Suarez, O.D., Peña-Pedraza, H.: Mie scattering study of dielectric nanoparticles and nanoantennas applications. Rev. Acad. Colomb. Cienc. Ex. Fis. Nat. 44(173), 974-983 (2020) DOI: https://doi.org/10.18257/raccefyn.1265

[16] Hagita, K.: Nanovoids in uniaxially elongated polymer network filled with polydisperse nanoparticles via coarse-grained molecular dynamics simulation and two-dimensional scattering patterns. Polymer. 174, 1016 (2014) DOI: https://doi.org/10.1016/j.polymer.2019.04.040

[17] Wang, Q., Xu, C., Jiang, Y., al.: The synthesis of conjugated polymers with different length side chains and the effect on their nanoparticles. AIMS Materials Science 5, 770-780 (2018) DOI: https://doi.org/10.3934/matersci.2018.4.770

[18] Rizvi, S.B.: Nanoparticle manufacturing: Challenges and opportunities. Biomaterials Research 23(1), 1-7 (2019) DOI: https://doi.org/10.1186/s40824-019-0176-1

[19] Castro, H.P., Pereira, M.K., Ferreira, V.C., al.: Optical characterization of carbon quantum dots in colloidal suspensions. Optical Materials Express 7, 401-408 15 (2017) DOI: https://doi.org/10.1364/OME.7.000401

[20] Sattar, T., Athar, M.: Nano bio-mofs: Showing drugs storage property among their multifunctional properties. AIMS Materials Science 5, 508-518 (2018) DOI: https: //doi.org/10.3934/matersci.2018.3.508

[21] Begines, B., Ortiz, T., Pérez-Aranda, M., et al.: Polymeric nanoparticles for drug delivery: Recent developments and future prospects. Nanomaterials 10 (2020) DOI: https://doi.org/10.3390/nano10071403

[22] O'Brien, G.: Nanoscale electronic properties of conjugated polymers and nanocrystals. PhD thesis, University College Cork, United States (2006)

[23] Matzler, C.: Matlab functions for Mie scattering and absorption. Technical report, IAP Res Rep. (2002)

[24] Mishchenko, M.: Electromagnetic scattering by nonspherical particles: A tutorial review. Journal of Quantitative Spectroscopy and Radiative Transfer 8 (2009) DOI: https://doi.org/10.1016/j.jqsrt.2008.12.005

[25] Aparicio, L., Ramos-Ortiz, G., Pichardo, J., et al.: Two-photon excited fluorescence of silica nanoparticles loaded with a fluorene-based monomer and its cross-conjugated polymer: Their application to cell imaging. Nanoscale 4 (2012) DOI: https://doi.org/10.1039/c2nr31925j

[26] Bohren, C.F., Huffman, D.R.: Absorption and Scattering of Light by Small Particles, 2nd edn., pp. 82-129. Wiley - VHC, New York (1983)

[27] Arfken, G.B., Weber, H.J., Harris, F.E.: Mathematical Methods For Physicists: A Comprehensive Guide, 7th edn., pp. 643-671. Academic Press, New York (2013) DOI: https://doi.org/10.1016/B978-0-12-384654-9.00014-1

[28] Martínez, J.: Determinación de tamaños de partículas mediante la dispersión angular de la luz. Master's thesis, University of Havana, Cuba (2006)

redalyc
UAEMEX

Available in:
https://www.redalyc.org/articulo.oa?id=91182133005

How to cite

Complete issue

More information about this article

Journal's webpage in redalyc.org

Scientific Information System Redalyc
Diamond Open Access scientific journal network
Non-commercial open infrastructure owned by academia

Agni Puentes Ossa, Diego Julian Rodriguez Patarroyo, Julian Andres Salamanca Bernal

Computational Modeling of Light Scattering in Polymer Nanoparticles for Optical Characterization*
Modelado Computacional de la Dispersión de Luz en Nanopartículas de Polímero para Caracterización Óptica
Modelagem computacional da dispersão da luz em nanopartículas de polímero para caracterização óptica

Ciencia e Ingeniería Neogranadina
vol. 34, no. 2, p. 63 - 75, 2024
Universidad Militar Nueva Granada,
ISSN: 0124-8170
ISSN-E: 1909-7735

DOI: https://doi.org/10.18359/rcin.7276